Experimental and numerical simulation of air-water two-phase flow in the rod bundle with grid spacer

WANG Xiao-Jun, CHEN Bing-De, HUANG Yan-Ping

(National Key Laboratory of Bubble Physics and Natural Circulation, P.O.Box 622-205, Chengdu 610041)

Abstract Experimental and numerical simulation were carried out on vertically upward air-water two-phase flow in the rod bundle with grid spacer. The related numerical simulation has been performed by using the Computational Fluid Dynamics code-CFX4.2, in which lateral interfacial effects based on a two-fluid model are accounted for. This model has been used to evaluate the velocity fields of gas and liquid phases, as well as phase distribution between elements in rod bundle by simulating 1/4 zone of experimental model, and mixing vanes of spacer in this area. Furthermore, this model has been used to predict the effects of spacer on flow and pressure drop along the rod bundle. The calculation results show that the mixing vane has significant influence on axial and lateral velocity. In order to obtain some experimental data to verify the numerical solutions, a series of tests, using a specially designed 3×3 rod bundle test section with AFA-2G structure spacer have been performed. An optical probe was used to measure local void fractions. At the same time, the pressure loss has been measured. A comparison between the calculated void profile and pressure loss and the measured results shows that the predicted void profiles are consistent at low gas apparent velocity. This research shows that the code CFX4.2 can be used to describe the 3-D air-water two-phase flow in the rod bundle channel with grid spacer.

Keywords Grid spacer, Air-water, CFX4 code, Optical probe, Two-phase flow

CLC number TL333

1 Introduction

Grid spacer is the key part of reactor fuel assembly. The presence of spacers in fuel assemblies affects various thermal-hydraulic characteristics of the reactor core. The grid spacer with fine performance can improve thermal-hydraulic performance of the core fuel assembly and enhance the critical heat flux without too much augment of the pressure loss. As a result, the implementation of grid spacer with high thermal performance provides more thermal margin, then increases safety level of the core. To study flow characteristics in the near-spacer region and find a new design tool for grid spacer, a series of researches have been carried out in National Key Laboratory of Bubble Physics and Natural Circulation-(BPNCL). The 3-D single phase flow field in rod bundles with grid spacers and the effects of grid structure on the flow have been studied by numerical solution with Computational Fluid Dynamics code CFX4.2 and visualized test.[1] In this paper, the test results and theoretical computation analysis of multi-dimensional air-water two-phase flows in rod bundle with grid spacer are presented.

Received date: 2002-09-09

2 Numerical simulation

2.1 Modeling

For the calculations, the two fluid model implemented in CFX4.2 is applied. The liquid phase is represented as continuous and the gas as disperse phase with a constant bubble diameter of 2.5 mm. The general form of the two-fluid model for adiabatic air-water flow can be written as:

$$\frac{\partial}{\partial t}\left(\beta_i\rho_i\right)+\nabla\bullet\left(\beta_i\rho_i U_i\right)=0 \qquad (i=l,g) \tag{1}$$

$$\frac{\partial}{\partial t}\left(\beta_i\rho_i U_i\right)+\nabla\bullet\left(\beta_i\rho_i U_i\times U_i\right)=\nabla\bullet\left[\beta_i\mu_i^e\left(\nabla U_i+\left(\nabla U_i\right)^T\right)\right] -\beta_i\nabla p_i+\beta_i\rho_i g_i+M_i \qquad (i=l,g) \tag{2}$$

The major interfacial forces are normally given by[2]

$$M_i = M_i^D + M_i^L + M_i^{Lw} + M_i^{TD} \qquad (i = l, g) \tag{3}$$

Drag force

$$M_l^D = -M_g^D = n_p M_p = \frac{3}{4} C_D \rho_l \beta_g \left| U_g - U_l \right| \times \left(U_g - U_l \right) \tag{4}$$

Lift force

$$M_l^L = -M_g^L = C_L \rho_l \beta_g \left(U_g - U_l \right) \times \left(\nabla \times U_l \right) \tag{5}$$

Turbulent dispersion force

$$M_l^{TD} = -M_g^{TD} = C_{TD} \rho_l k_l \nabla \beta_g \tag{6}$$

The "lubrication" force

$$M_l^{Lw} = -M_g^{Lw} = C_{Lub} \beta_g \rho_l \frac{\left| U_g - U_l \right|^2}{d} n_w \tag{7}$$

For the coefficient

$$C_{Lub} = \max\left(0, C_{w1} + C_{w2} \frac{d}{y_w} \right) \tag{8}$$

Two-phase flow turbulence is normally modeled by using the *k*-ε model for the continuous liquid field (i=l), and modified to include the effect of bubble-induced turbulence (Sato model). The effective turbulence viscosity for the liquid can be written as follows:

$$\mu_l^e = \mu_l + \rho_l C_\mu \frac{k_l^2}{\varepsilon_l} + C_{\mu b} d \rho_l \beta_v \left| U_v - U_l \right| \tag{9}$$

The turbulent kinetic energy (*k*) and the turbulent energy dissipation (ε) are calculated by a conventional *k*-ε model.

The effective turbulence viscosity for the gas can be written as follows:

$$\mu_g^e = \mu_l^e \frac{\rho_g}{\rho_l} \tag{10}$$

2.2 CFX4.2 calculation

AFA-2G 3×3 grid spacer and a rod bundle were modeled. The calculations were performed by simulating 1/4 zone of the test channel which is shown in Fig.1 and mixing vanes of grid spacer in this area. The transversal modeling region and elements are shown in Figs.2 and 3. The axial modeling region includes 4 rods and one grid spacer, and begins at 50 mm upstream of grid spacer. The axial total length is 515 mm.

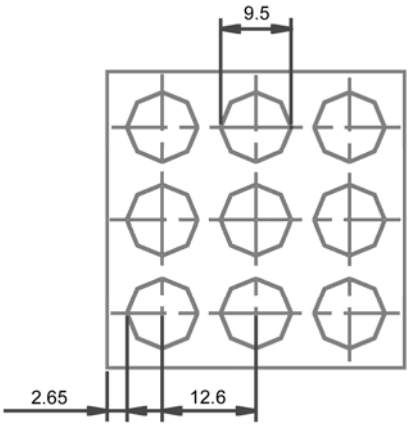

Fig.1 Diagram of the test channel.

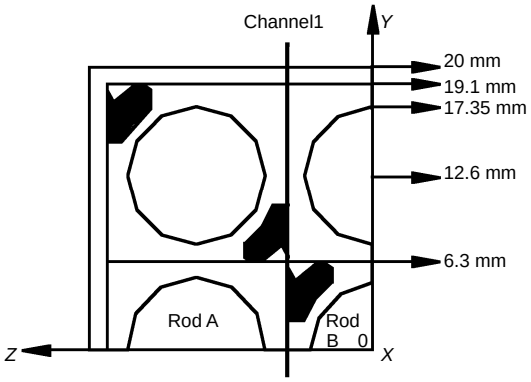

Fig.2 Transversal modeling region.

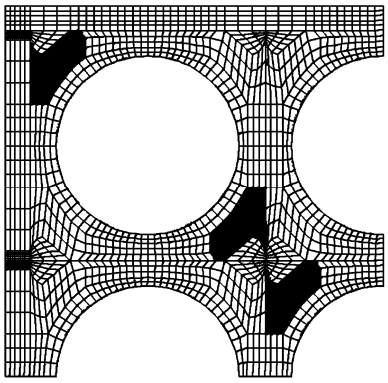

Fig.3 Transversal modeling elements.

During the present calculations, the flow for both phases was modeled as turbulent. On the wall, a non-slip for the liquid phase and a free-slip boundary

condition for the gas phase were set. A fluid velocity profile at the inlet according to a fully developed single phase fluid flow and section void models was given. At the outlet on the top of the rod bundle, a pressure boundary condition was set. The spacer and its mixing vane were treated as infinite thin surfaces in the model and a zero velocity condition and turbulent wall function were applied on each side of the thin surfaces. The finite-volume method was adopted to obtain the discrete equations. The upwind differencing was chosen for the volume fraction. The central differencing was chosen for the pressure. The default difference schemes were used for the rest. The velocity-pressure coupling algorithm was based on the updated SIMPLE algorithm (SIMPLEC). The inter-phase slip algorithm (IPSA) was applied for the inter-phase transport terms coupling.

2.3 Computational results and discussions

2.3.1 Influence of interfacial force

There are several inter-phase non-drag forces in CFX4.2, which are lift force, wall lubrication force and force induced by turbulence. All of these forces would be discussed in turn.

a. Lift force

C_L is lift force coefficient, which can take values between 0.01and 0.05 for weak viscous flow. The analysis of sensibility for lift force coefficient has been performed by taking values 0.01, 0.02 and 0.03 respectively. The calculational results show that the prediction was failed when its value was more than 0.03. The result shows that the volume fractions near rod wall and channel wall increase rapidly with lift force. The volume fraction peak near wall will also increase as the lift force coefficient increases.

b. Turbulent dispersion force

When only the turbulent dispersion force is considered for non-drag forces, because of the turbulence, the volume fractions from the center of center channel to near wall decrease sharply. The result shows that the turbulent dispersion force acts on the whole region and the distribution of the volume fraction in the flow region is more complanate due to the effect of the turbulent dispersion force.

c. “Lubrication” force

When only the “lubrication” force is considered for non-drag forces, the “lubrication” force makes the volume fractions near wall decrease.

If the three non-drag forces are all considered, the result is almost the same as when only the turbulent dispersion force is considered for non-drag forces. It means that the turbulent dispersion force has an important influence on the distribution of the volume fractions.

2.3.2 Influence of different void model

It is necessary to provide initial velocity for inlet at the beginning of calculations. To obtain ideal initial velocity in two-phase flow as in the single phase flow, the section void fraction of inlet must be known. For the rod bundle channel, currently idealized model is absent. In this prediction, three models, i.e. Miropoliski empirical formula, Armand empirical formula[3] and homogeneous model, have been performed. The volume fractions calculated by Miropolisky empirical formula are higher and the volume fractions calculated by homogeneous model are lower, but their trends are the same.

2.3.3 Influence of bubble size

The bubble size is assumed to be a constant during the calculations. The sensibility analyses for bubble diameter have been performed by taking values 0.6 mm, 1.5 mm and 3 mm respectively. The results show that the volume fraction peaks decrease appreciably with the bubble size augmenting. In general, the code is not dependent on the bubble size.

2.3.4 The influence of grid spacer

Fig.4 shows the distributions of volume fractions at the different cross sections with or without grid spacer. Without spacer, the volume fractions at the center channel are little. With spacer, the volume fractions at the center channel increase sharply because of the presence of mixing vane. Far from spacer, the mixing effect of the vane becomes weak and the volume fractions at the center channel decrease. Because the grid spacer makes the volume fractions at the center region of the sub-channel increase, the volume fractions near wall will decrease and the thermal performance of the rod wall would be improved.

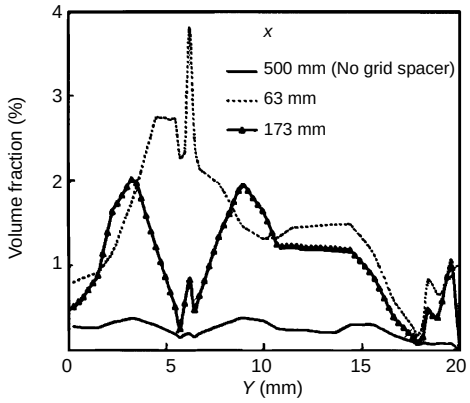

Fig.4 Influence of grid spacer.

3 Experimental researches

3.1 Test facility and methods

Fig.5 is a schematic diagram of the test facility used in present study. Water is circulated by a pump from a storage pool through a Venturi meter into the test section and then mixed with the air, metered by a float flowmeter to generate a two-phase flow. The air flows into the mixing zone, located upstream of the test section, through 0.6 mm diameter holes drilled at a hollow cylinder. Two-phase mixture flows vertically upward in the rod bundle and then returns into the storage pool. The temperature and pressure of air and water are measured near the test section inlet by thermocouples and pressure transducers. The pressure difference between the measuring points on the test section is measured by a differential pressure transducer.

The test section mainly consists of 3×3 rod bundle with AFA-2G grid spacer. The rod bundle consists of nine 9.5 mm diameter rods arranged in a square with 12.6 mm pitch. The rod bundle hydraulic diameter is 8.98 mm. The gap of rod to wall is 2.65 mm.

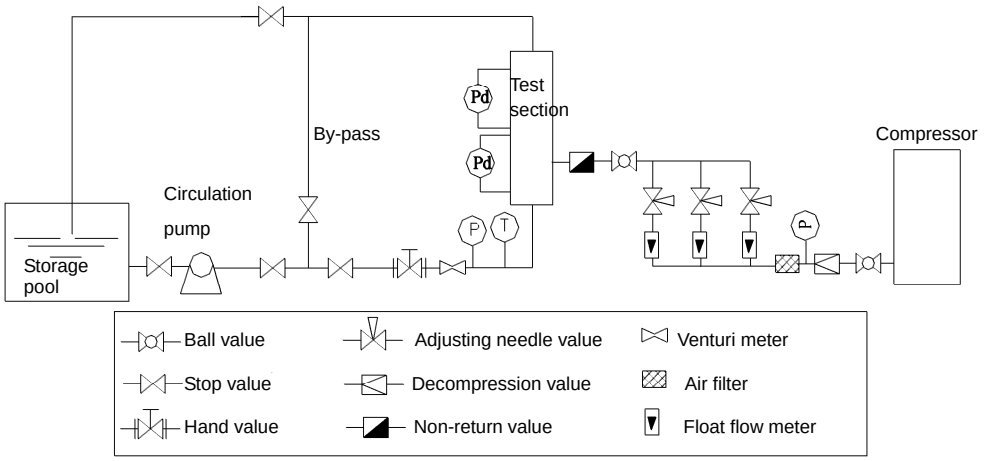

Fig.5 Schematic diagram of the test facility.

The RBI optical probe system consisting of optical probe, optroelectronic module, acquisition and signal processing, calculation and display software was used to measure void fraction. To obtain the initial real-time signal of probes, a numerical HP54600B dual-trace oscilloscope was added to the measurement system. The local void fractions were measured at two cross sections, 30 mm and 140 mm downstream of the grid spacer, depicted in Fig.6. There are 12 transversal measuring points, locating at channel 1 depicted in Fig.2, the distances to the *z* axis are 0 mm, 2.0 mm, 3.5 mm, 5 mm, 6 mm, 7 mm, 7.5 mm, 9 mm, 10 mm, 11.5 mm, 13 mm and 14 mm respectively. The sampling time is about 10 to 30 s. At the same time, the pressure loss of rod bundle and spacer under one-phase and two-phase flow conditions had been measured. All experiments were conducted using air and water at room temperature.

3.2 Experimental results and discussions

In general, the ideal signal should be square wave. The high level signal/ low level signal express gas/liquid phase of local points respectively. However, in the actual measurements, it is very important to select the proper threshold signal level for improving accuracy of measurement because the actual signal

mixes noise signal. In this study, horizontal threshold is adopted. The sensibility analyses for threshold signal level have been performed for two probes, depicted in Fig.7. When the threshold signal level is between 1.4 V and 3.3 V, the variation of the void fraction measured by probe is smaller, so the threshold signal levels of the two probes are selected as 1.4 V.

Figs.8~10 shows the distributions of the void fraction under the conditions of different air flow rate, different water flow rates and the same volume void fractions. In Fig.8, the void fractions in the measuring channel increase with the air flow rates increasing. The form of the distribution curve at the same cross section is almost consistent, but the distribution curve is more complanate at the lower air flow rate. The distribution curves at two cross sections are different, the void fraction at the sub-channel center region is higher distinctly than that near the wall at the upstream channel, both of which are reverse at the downstream channel, and the void fraction far from spacer channel is almost higher than that near spacer channel at the same transverse positions. Because the grid spacer has mixing vanes to promote the water mixing around rods, it makes the gas bubble have the trend of moving toward the sub-channel center. The mixing decreases as going to downstream. In Fig.9, the void fractions in the measuring channel decrease with the water flow rates increasing. But when the water flow rate decreases to a certain value, the distribution will change. At the same time, the slug flow occurs at most positions of the measuring channel. The flow patterns change, and the distributions of the void fraction will also change. In Fig.10, the distributions of the void fraction near spacer are very different at the same cross section in the conditions of the same volume fractions due to mixing of vanes, and thus the flow characteristics are also different. So it is very necessary to know the two-phase flow characteristics near spacer. But the distribution trend far from spacer is nearly the same with weak effect of the grid spacer. It can be found that the grid spacer has great influence on the two-phase distribution.

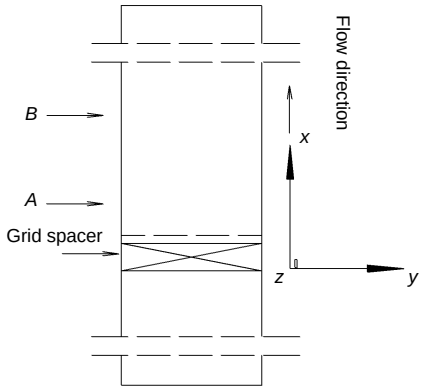

Fig.6 Axial measured point distribution.

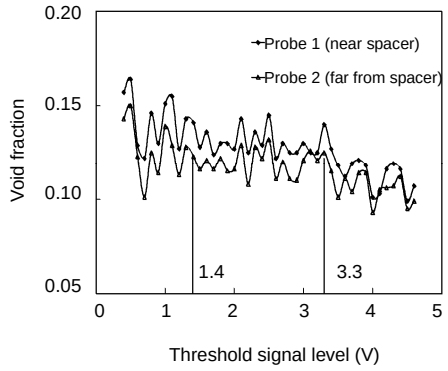

Fig.7 Sensibility analyses for threshold signal level.

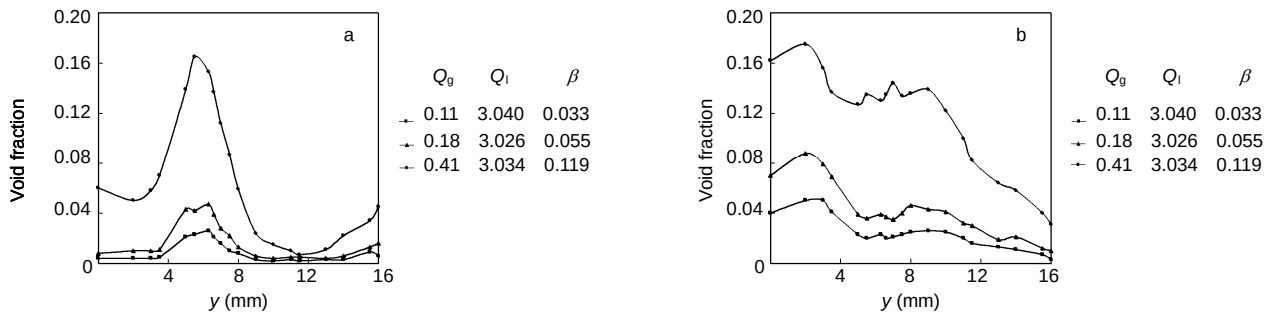

Fig.8 (a) Distributions of the void fraction 30 mm downstream of the grid spacer; (b) Distributions of the void fraction 140 mm downstream of the grid spacer.

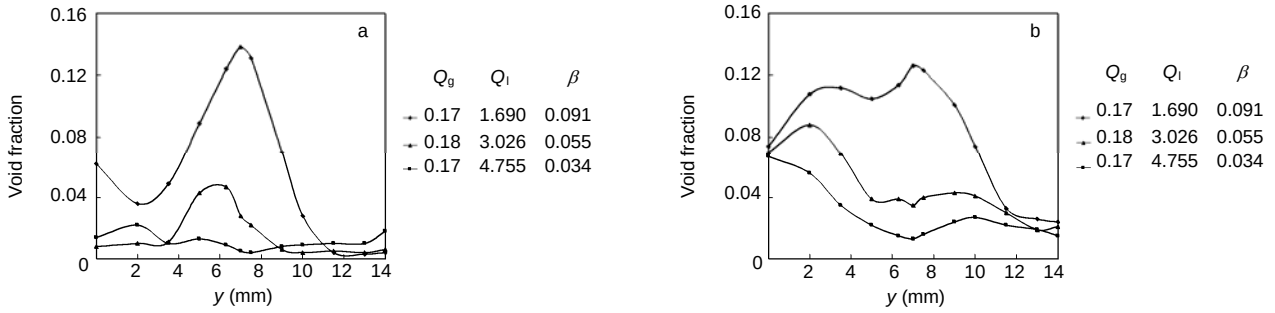

Fig.9 (a) Distributions of the void fraction 30 mm downstream of the grid spacer; (b) Distributions of the void fraction 140 mm downstream of the grid spacer.

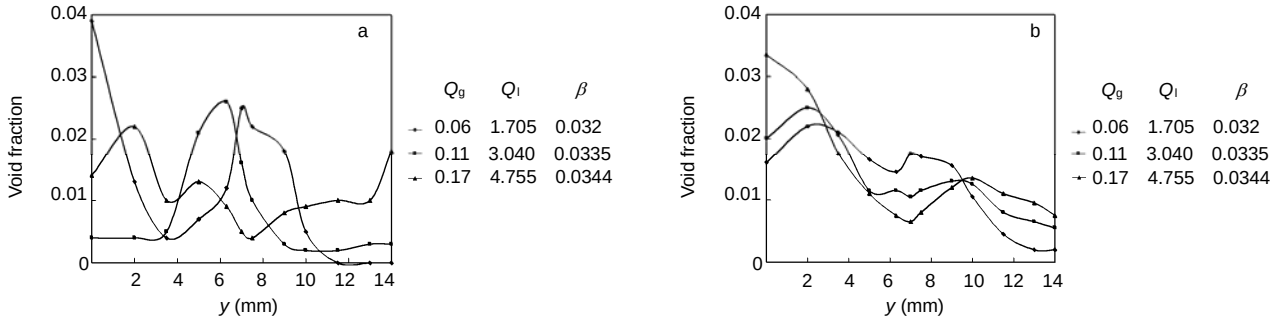

Fig.10 (a) Distributions of the void fraction 30 mm downstream of the grid spacer; (b) Distributions of the void fraction 140 mm downstream of the grid spacer.

4 Verification of predictions

The measurement and the CFX4.2 calculation of the two-phase pressure loss of bare bundle in 8 different test conditions are shown in Fig.11. Evaluations of the pressure loss are underestimated at the low mass fraction less than 2.53×10^{-4}. The prediction increases as the mass fraction increases. When the mass fraction reaches to 2.53×10^{-4}, the prediction will even be overestimated. It might be caused by the drag force coefficient model. But the differences of calculation and measurement are all within $\pm12\%$, the mean deviation is about 5.11%. It means that the numerical simulation for two-phase flow in the channel is valid.

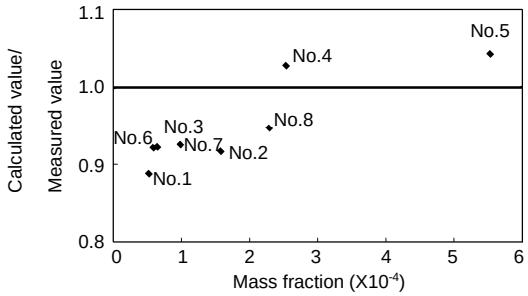

Fig.11 Comparison of the pressure loss.

The comparison between the calculated and measured void fractions at 30 mm downstream of the grid spacer is shown in Fig.12. The liquid water superficial velocity is 0.87 m/s. The gas air superficial velocity for different tests increases from 0.032 to 0.12 m/s. It can be observed that the CFX4.2 code can predict approximately the air-water two-phase flow in the bundle with grid spacer in the conditions of low volume fractions. But in the conditions of higher volume fractions, the predictions are in poor agreement with the measurements. With the gas velocity increasing, the void fraction at the center sub-channel is underestimated while that at the side sub-channel is overestimated. The reason might be found in the occurrence of bubble coalescence and bubble diffraction effect, which are not considered in the models. In fact, the bubble diameter is not a constant in two-phase flow. Larger bubbles having dimensions in the order of the sub-channel diameter will be exposed to other bubble forces than here modeled. At the same time, the reduction of the simulating structure might bring some calculational deviations also.

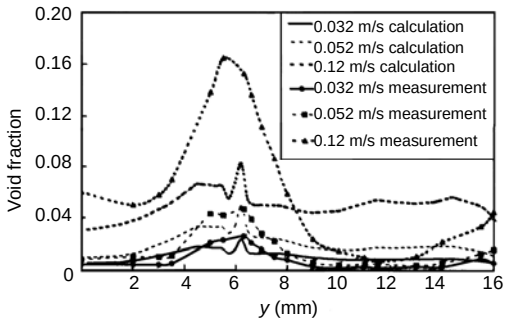

Fig.12 Comparison between the calculated and measured void fractions.

5 Conclusions

The numerical simulations for air-water two-phase flow in the 3×3 rod bundle with AFA-2G grid spacer have been performed by using a Computational Fluid Dynamics code CFX4.2, and the results have been verified by the test. The comparison of the results shows that the numerical simulation for bubbly air-water two-phase flow in rod bundle with spacer is valid. The CFX4 can predict the structural effect on the flow field, so the applicability of the CFX4.2 code evaluation method for the design of the grid is confirmed. The method can be used to analyze initially bubbly two-phase flow in complicated channel. However the investigated tests show the limits of the assumption of a single bubble diameter. Model extensions which consider the bubble diameter distribution and model bubble coalescence and bubble diffraction effect would be necessary. The results should provide the basis for further researches on steam-water two-phase flow and heat transfer, as well as critical heat flux of the rod bundles with grid spacers.

Nomenclature

C_{μ}, $C_{\mu b}$: constants in Eq.(9)

C_D: drag force coefficient

C_L: lift force coefficient

C_{Lub}: “lubrication” force coefficient

C_{w1}, C_{w2}: coefficients in Eq.(8)

C_{TD}: turbulent dispersion force coefficient

M_i: interfacial force per unit volume for phase i, $kg\cdot m^{-2}\cdot s^{-2}$

M_i^D: drag force, $kg\cdot m^{-2}\cdot s^{-2}$

M_i^L: lift force, $kg\cdot m^{-2}\cdot s^{-2}$

M_i^{Lw}: “lubrication” force, $kg\cdot m^{-2}\cdot s^{-2}$

M_i^{TD}: turbulent dispersion force, $kg\cdot m^{-2}\cdot s^{-2}$

U_i, U_l, U_g: velocity of phase i, liquid and gas , respectively, $m\cdot s^{-1}$

d: bubble diameter, m

k_l: turbulent kinetic energy, m^2s^{-2}

n_w: unit vector normal to a wall

p_i: pressure, Pa

t: time, s

y_w: distance to a wall, m

β_i, β_g: volume fraction of phase i and gas, respectively

ε_l: dissipation of turbulent kinetic energy, $m^2\cdot s^{-3}$

μ_l: molecular viscosity of liquid, $kg\cdot m^{-1}\cdot s^{-1}$

μ_l^e, μ_g^e: effective viscosity of liquid and gas, $kg\cdot m^{-1}\cdot s^{-1}$

ρ_i, ρ_l, ρ_g: density of phase i, liquid and gas,respectively, $kg\cdot m^{-3}$

References

1 Xiong W Y. 3-D flow field studied in rod bundles with spacer grids, Internal report, not published

2 CFX4.2 Flow solver user guide

3 Collier J G, Thome J R. Convective boiling and condensation, 3rd ed., Clarendon Press, Oxford, 1994